Hot-carrier and optical-phonon ultrafast dynamics in the topological insulator Bi_2Te_3 upon iron deposition on its surface

M. Weis,[1,2,*] K. Balin,[1] B. Wilk,[1] T. Sobol,[1,3,4] A. Ciavardini,[4,5] G. Vaudel,[2] V. Juvé,[2] B. Arnaud,[2] B. Ressel,[5,6] M. Stupar,[5,6] K. C. Prince,[6] G. De Ninno,[5,6] P. Ruello,[2,†] and J. Szade[1,3,‡]

[1]*A. Chełkowski Institute of Physics, University of Silesia, 41-500 Chorzów, Poland*

[2]*Institut des Molécules et Matériaux du Mans, UMR 6283 CNRS, Le Mans Université, 72085 Le Mans, France*

[3]*National Synchrotron Radiation Centre SOLARIS, Kraków, Poland*

[4]*Central European Research Infrastructure Consortium, CERIC-ERIC, 34149 Trieste, Italy*

[5]*University of Nova Gorica, SI-5000 Nova Gorica, Slovenia*

[6]*Elettra Sincrotrone Trieste, I-34149 Trieste, Italy*

(Received 22 July 2021; accepted 15 November 2021; published 6 December 2021)

Topological insulators (TIs) are promising materials for future spintronic applications such as emerging spin-to-charge conversion (SCC) devices, possibly working at GHz-THz frequency for ultrafast data processing. These devices will rely on hybrid nanostructures composed, for example, of a ferromagnetic layer deposited on the topological insulator. The efficiency of spin-to-charge conversion will depend on the quality of the interface, including chemical (interfacial chemical reactions) and physical (band bending effect, Fermi pinning) aspects. This paper presents a complete study of electronic structures and photoexcited carrier dynamics in topological insulators capped with iron and iron oxide. We combine static and time-resolved angle-resolved photoemission spectroscopies (ARPES, TR-ARPES) with time-resolved optical methods (transient optical reflectivity and transmission). Both single crystal and thin films of Bi_2Te_3 are studied. We show that monolayers of iron and iron oxide significantly affect the electronic band structure at the interface by shifting the Fermi level into the conduction band, which we explain by a band bending effect, and is confirmed by *in situ* XPS measurements. This modified interfacial electronic structure offers a new channel for relaxation of hot carriers, illustrated by a drastic decrease of their characteristic decay time after optical excitation. These results might have a potential impact in the future development of TI-based SCC devices.

DOI: 10.1103/PhysRevB.104.245110

I. INTRODUCTION

Topological matter has taken a central position in solid state physics during the last decade. Various topological phases such as three-dimensional (3D) topological insulators (TIs), Weyl semimetals, quantum spin Hall insulators, and quantum anomalous Hall insulators have been studied [1–3]. Surface states and their spin-momentum locking give rise to many different interesting spin-related physical phenomena. The study of topological insulators has entered the stage of finding the best possible systems to harness their unique properties. Among very promising applications for spintronic devices, the spin-charge-conversion (SCC) process has attracted particular attention [4–7]. In the case of TI-based systems, this conversion process is based on the inverse-Edelstein effect (IEE) [4,5] which corresponds to conversion of a spin current, usually generated in a ferromagnetic (FM) layer and impinging with a normal incidence on a FM-TI interface (injection of spin current in the surface Dirac states), into a transversal charge current in the TI layer or at the interface of the FM-TI layers. The figure of merit of the IEE is given by a characteristic distance (λ_{IEE}) which depends, using a phenomenological approach [6], on the product of the Fermi velocity on the Dirac cone with a characteristic time [4–6]. That characteristic time involves the spin tunneling time at the interface and the spin relaxation time (including the effect of defects and roughness) [4,5]. Longer time corresponds to a better figure of merit. That time depends on the electronic band structure formed at the junction between a FM material and the TI. Consequently, it becomes essential to characterize the interfacial electronic structure and to know the relaxation channels of out-of-equilibrium carriers and spin in such hybrid nanostructures.

Surface and bulk carriers dynamics in bulk [7–16] or thin films [17–20] have been investigated in detail during the last ten years, either with photoemission [9–16] or with optical techniques [7,8,17–20]. Channels of carrier relaxation between surface and bulk states have been discussed, and Dirac electron relaxation times ranging from picoseconds to hundreds of picoseconds [12,14,15] and even up to microseconds [13] were reported, illustrating the complexity and the richness of the dynamics. The carrier dynamics, sometimes probed by time-domain THz spectroscopy [21], can also be influenced by the surface band bending and associated Schottky effect as evidenced recently [7]. In the case of ultrathin films of TIs consisting of a couple of quintuple layers, drastic

*Current address: Laboratoire d'Optique Appliquée, ENSTA, CNRS, Ecole Polytechnique, 91761 Palaiseau, France.

†pascal.ruello@univ-lemans.fr

‡jacek.szade@us.edu.pl

confinement effects, where surface state hybridization occurs, lead to an opening of a gap at the Dirac cone as well as a modification of the bulk gap [22–24]. Subsequent significant evolution of the lifetime of above band-gap photoexcited carriers has been reported in several works [18–20]. Beside these studies of pure TIs, the experimental description of the carrier dynamics at short time scales in hybrid FM-TIs has been investigated experimentally only recently in hybrid Co/Bi_2Se_3 nanostructures [7], while several theoretical works have been carried out to describe the electronic properties [25] and the SCC [5,6] in hybrid nanostructures. Although promising for future spintronic devices, realization of such hybrid nanostructures requires an understanding of the interaction between the deposited layer and the topological insulators including both physical and chemical aspects at the interface. The deposition of a FM layer can indeed lead to several effects such as breaking the Dirac cone through a magnetic interaction [25], surface state creation due to atomic diffusion [26], Fermi level shift by surface doping [27,28] in relation to junction effects [25,27]. It has been theoretically predicted that the proximity effect of FM layers is more complex than the effect of a pure magnetic exchange breaking of the time-reversal and electronic hybridization in doped bulk TIs. Furthermore, some smearing out of TI states at interfaces has been predicted [25] which might drastically affect many physical properties.

In this paper, we evaluate how the photoexcited carrier and phonon dynamics in Bi_2Te_3 (bulk and thin films) materials are influenced by the proximity of an ultrathin layer of a magnetic metal, Fe, or a magnetic insulator, Fe_2O_3. We combine both static and time-resolved angle-resolved photoemission spectroscopy (i.e., ARPES and TR-ARPES), sensitive to surface states, with time-resolved optical pump-probe spectroscopy (transient reflectivity, TR, and transient transmission, TT) integrating the surface and bulk responses. We show that the proximity of iron and iron oxides shifts the Fermi level into the conduction band (CB) via a band bending effect, revealed by both ARPES and by a detailed analysis of XPS spectra. This leads to a drastic decrease of photoexcited carrier relaxation time by a factor close to 2 for 0.4 monolayer of iron (ML) on bulk Bi_2Te_3 and up to a factor of 5 for thin films covered by 1 nm of iron oxide. These observations strongly support the existence of new channels of relaxation for photoexcited carriers that resemble a fast intraband relaxation process similarly to metallic systems. Such drastic behavior of the transient dynamics is observed for carriers in the bulk bands, but we cannot confirm directly the same behavior for the Dirac states at this stage due to limited resolution of the TR-ARPES.

Finally, although we do not probe directly the spin transmission at the interface and the SCC efficiency, these results provide some relevant information about electron and phonon dynamics at the interface to guide the realization of hybrid nanostructures for SCC devices based on TIs since they address specifically the carrier dynamics at interfaces between the FM material and the TI.

II. EXPERIMENTAL METHODS

A. Samples and characterization

In this work we studied, in vacuum, a single crystal of Bi_2Te_3, with and without a capping layer of iron (Fe) or iron oxide (Fe^{+3}). We also studied, in air, thin films of Bi_2Te_3 grown on mica, either naturally passivated or with a capping layer of iron oxide (Fe^{+3}). An artistic view of all samples under investigation is shown in Fig. 1 within the Supplemental Material [29]).

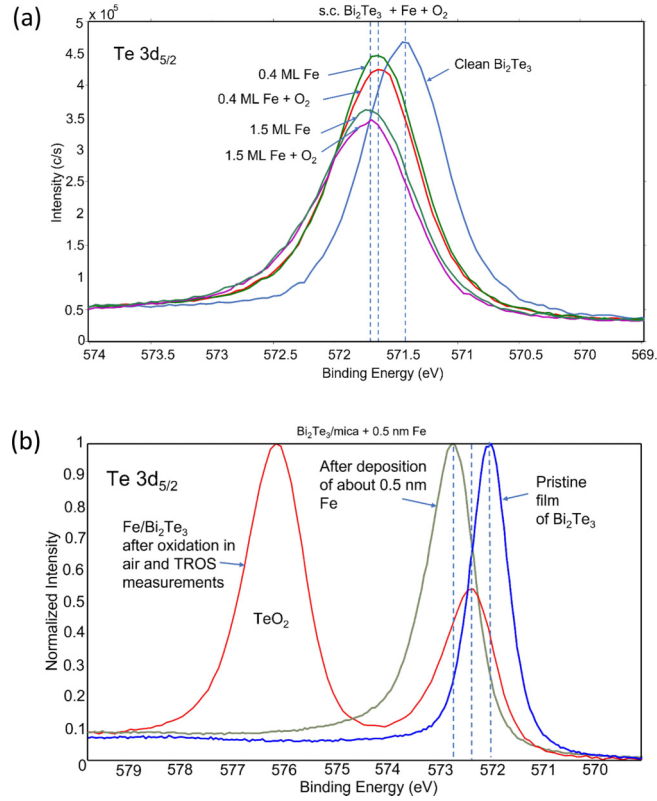

FIG. 1. (a) Set of XPS Te $3d_{5/2}$ spectra from a clean Bi_2Te_3 crystal and for the crystal capped with Fe and oxidized *in situ*. (b) XPS Te $3d_{5/2}$ core level line measurements for as deposited BT film and BT film capped with 0.5 nm of Fe. In red, measurements of the Te core level for the same film after oxidation (passivated) in air. Despite the oxidation, we note that the band bending, although a little reduced, persists for both the single crystal and thin film surfaces.

The single crystal of BT was supplied by MaTeck and had a size of $10\times10\times1$ mm^3. The crystal was divided into two parts. One was used for the measurements of the clean and Fe-capped Bi_2Te_3(001) crystal performed at the UARPES beamline at the synchrotron SOLARIS. The other part was used for TR-ARPES measurements performed at the Laboratory of Quantum Optics of the University of Nova Gorica. In both cases, the crystal was exfoliated in UHV just before the measurements. The Fe film was deposited from an electron beam evaporator. The thickness was controlled by the deposition time and it was measured by using a quartz balance for UARPES measurements and by XPS measurements for TR-ARPES. A thickness less than 1 monolayer means that there is most likely a statistical distribution of adatoms on the surface. For the TR-ARPES, a study of a controlled oxidized surface was performed by dosing O_2.

The photoelectron spectrometer used for TR-ARPES was also used for XPS analysis using monochromatic Al Kα radiation. The spectra of the BT crystal, exfoliated and after Fe

evaporation on the exfoliated surface, was measured in the regions of the C 1s and O 1s core levels. No contamination with carbon or oxygen was found before or after Fe deposition. The variation of intensity of photoemission lines before and after Fe deposition was used to estimate the thickness of the Fe layer. Exponential damping of the photoelectron intensity was assumed and the inelastic mean free path of photoelectrons was calculated with the use of the QUASES software [30].

The thin films of Bi_2Te_3 were deposited on muscovite mica substrates in a molecular beam epitaxy chamber (Surface Physics Laboratory of the University of Silesia, Chorzów). Details of the topological insulator thin film growth and characterization (reflection high-energy electron diffraction, RHEED, low-energy electron diffraction, LEED, and x-ray photoelectron spectroscopy, XPS) were described in our previous papers [17,19,26,31]. After depositing the monocrystalline layer of Bi_2Te_3, we deposited on half of the sample an ultrathin layer of iron. We also studied a wedgelike structure whose iron layer thickness, deposited onto the BT film, gradually changes from 0 to 1 nm (see Supplemental Fig. 1 [29]). The BT films under investigation are rather thick (15 nm) and, without iron on the top surface, behave as bulk materials and do not exhibit a confinement effect as discussed recently [19]. *In situ* XPS measurements were conducted to analyze the core levels of the BT films with and without the iron capping layer and details of the electronic structure are discussed below.

B. Continuous and time-resolved spectroscopic methods

Angle-resolved photoemission spectroscopy measurements were performed at the UARPES beamline at the synchrotron SOLARIS. The photon source was the EPU quasiperiodic undulator. Measurements were carried out in ultrahigh vacuum of about 1×10^{-10} mbar with the Scienta DA30L analyzer of the beamline and with horizontal *s* light polarization. All ARPES measurements were performed at 80 K. Fe was deposited from an electron beam evaporator at room temperature at the rate of 0.1 Å/min.

Time and angle resolved photoelectron spectroscopy measurements were performed at the Laboratory of Quantum Optics of the University of Nova Gorica. The setup consists of a HHG source (high harmonic generation), powered by an intense 800 nm Ti:sapphire laser producing 40 fs pulses with a 5 kHz repetition rate, 3 mJ per pulse [32]. Two thirds of this energy is used for generating the VUV probe pulse and one third is used as the IR pump pulse. For the TR-ARPES studies presented here, we used HHG radiation produced in argon with photon probe energy of 17.07 eV (72.6 nm, 3.10^7 photons/pulse). We used the 11th harmonic as it exhibited the highest flux. Either a *p* or *s* polarization was employed for the photon energy. The VUV radiation was monochromatized by a grating stage in the off-plane geometry for ultrafast time resolution, described in detail previously [33]. The monochromator transmitted 17.0 eV photons with 100 meV bandwidth. The pump wavelength we used was 800 nm with energies ranging from 1.5 to 2.2 μJ/pulse corresponding to a fluence of 0.9 to 1.3 mJ cm^{-2}. The pump and the probe beams impinged on the sample in an almost collinear geometry in order to minimize the temporal spread due to the lateral spot dimensions. The experimental chamber includes a commercial hemispherical Scienta R-3000 electron spectrometer coupled to the laser system. The time-resolved optical measurements were conducted at the Institut des Molécules et Matériaux du Mans (IMMM). A two-color pump-probe scheme was used with a 80 MHz repetition rate Ti:Sapphire laser and a synchronously pumped optical parametric oscillator (OPO); details of experimental parameters can be found in previous papers [17,19,31]. In our experiments we used a laser pump with wavelength 830 nm (1.49 eV) and a probe beam with a wavelength of 580 nm (2.14 eV) obtained with the synchronously pumped optical parametric oscillator. The typical fluences were between 30 and 100 $\mu J\,cm^{-2}$; for Bi_2Te_3 we previously observed linear optical response for this typical fluence range [19]. Both transient optical reflectivity and transmission were performed with different configurations where the pump light impinges either on the iron oxide/BT side (front configuration) or on the transparent mica substrate first before interacting with the BT layer side (back configuration).

Even though the probe energy is close to the optical absorption threshold of α-Fe_2O_3 [34] or of γ-Fe_2O_3 [35], the light absorption remains negligible considering that the oxide layers are ultrathin (<1 nm) compared to the optical skin depth, which we estimate to be around 40–50 nm for a wavelength of 550 nm for α-Fe_2O_3 [34]. Thus our pump and probe beams were highly transmitted through the iron oxide layer, and the excitation and detection processes were generated mainly within the layer of Bi_2Te_3. We also performed experiments with a pump excitation at 2.98 eV, i.e., well above the band gap of iron oxides and we drew similar conclusions, confirming the negligible contribution of the iron oxide in the measurement.

III. RESULTS AND DISCUSSION

A. XPS at thermodynamic equilibrium

XPS spectra of the specimens were measured and enabled us to understand the electronic structure of uncapped and capped materials (single crystal and thin films). For the single crystal, we found a shift of the Te and Bi core levels towards higher binding energy of 0.1–0.3 eV as a result of Fe deposition. The Te $3d_{5/2}$ line is shown in Fig. 1(a) (see Supplemental Fig. 2 in the Supplemental Material [29] for the Bi $4f_{7/2}$ line). The effect can be attributed to band bending [36] and will be further discussed together with the electronic structure resolved with ARPES. Note that the XPS spectra show the existence of a slight chemical reaction of Fe with the BT crystal at room temperature, which we attribute to the reaction of Fe with Te [26] probably leading to the formation of FeTe and the appearance of metallic Bi (see Supplemental Figs. 2 and 3 [29]). No specific signature was found for the Te 3*d* XPS doublet since the binding energy of the Te 3*d* line is equal for FeTe and for Bi_2Te_3. The analysis of the Fe 2*p* doublet was difficult due to the low intensity but we can confirm the Fe is metallic (see Supplemental Fig. 4 [29]). No evidence of Te or Bi oxides was found after *in situ* oxidation. Finally, the core level shift after this oxidation is similar to that observed with pure iron as shown in Fig. 1(b).

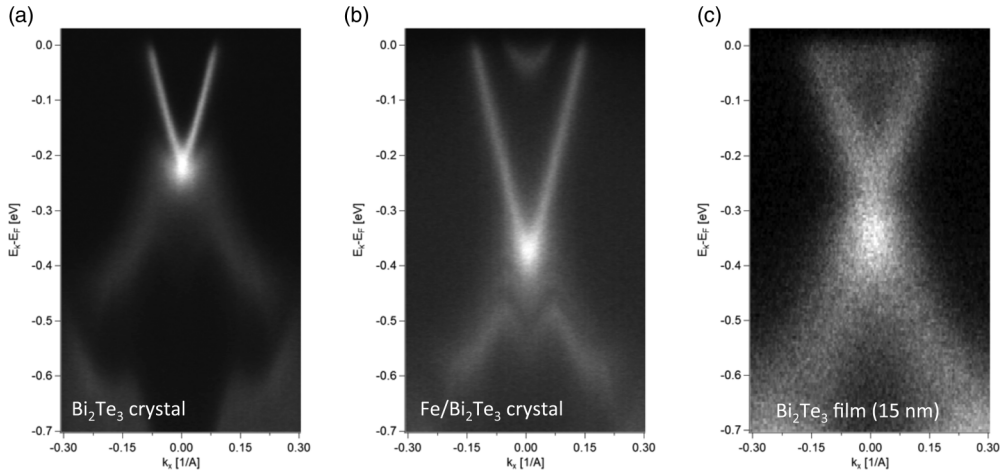

FIG. 2. ARPES band structure for a single crystal and a thin film measured at the UARPES beamline with a photon energy of 50 eV and an *s* polarization. (a) Signal at 80 K for a crystal with a clean surface, and (b) covered by a 0.2 ML of Fe. (c) ARPES signal of a BT film (15 nm) measured at 85 K. The horizontal axis is the momentum along the ΓK direction of the Brillouin zone.

For the thin films, for an iron capping layer of 0.5 nm, we observe the same shift of the Te $3d$ [Fig. 1(b)] and Bi $4f$ (Supplemental Fig. 5 [29]) lines towards higher binding energy that we also ascribe to a surface band bending. Once oxidized in air, some oxides are formed such as TeO_2 as shown in Fig. 1(b), and also Fe_2O_3 and Te and Bi oxides, as clearly revealed in Supplemental Figs. 6 and 7 [29]. Note that these oxides were not detected for the BT crystal covered by oxidized iron [see Fig. 1(a)] because the amount of iron was smaller than the one covering the film. Under such oxidation, the Bi $4f$ and Te $3d$ levels of the thin film still exhibit an energy shift indicating that the electronic structure of BT at the interface preserves a band bending: ∼0.2 eV for the Bi $4f_{7/2}$ level (Supplemental Fig. 5 [29]) and ∼0.3 eV for the Te $3d_{5/2}$ levels [Fig. 1(b)]. Depth profiling of the core level lines was performed for the films capped with a 2 nm thick iron layer. That sample was naturally oxidized in air (Supplemental Fig. 8 [29]). The spectra show the presence of iron oxide (Fe^{3+}) and some pure iron at the interface with BT and possibly some slight diffusion of iron into capped BT films.

B. ARPES at thermodynamic equilibrium

The band structure of the UHV exfoliated BT crystal measured at 80 K is shown in Figs. 2(a) and 2(b). The energy dispersion curves for the clean BT and the BT capped with 0.2 ML Fe for the energy region close to the Fermi level are compared. The clean single crystal of BT is of *n* type with the Fermi level below the bottom of the conduction band, crossing the Dirac cone. After deposition of about 0.2 ML Fe, the Fermi level is shifted by about 100 meV and enters into the conduction band which begins to be occupied by carriers. A similar effect was recently shown by Scholz [28] confirming the donor effect when an iron ML are deposited.

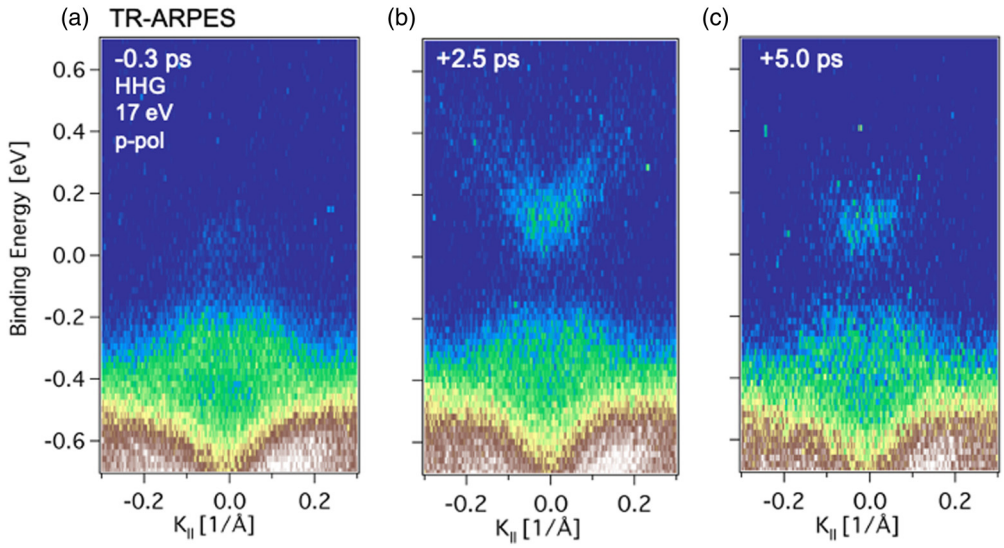

FIG. 3. The valence band structure of a Bi_2Te_3 single crystal as visible in TR-ARPES before the 800 nm optical excitation −0.3 ps (a) and after 2.5 ps (b) and 5 ps (c).

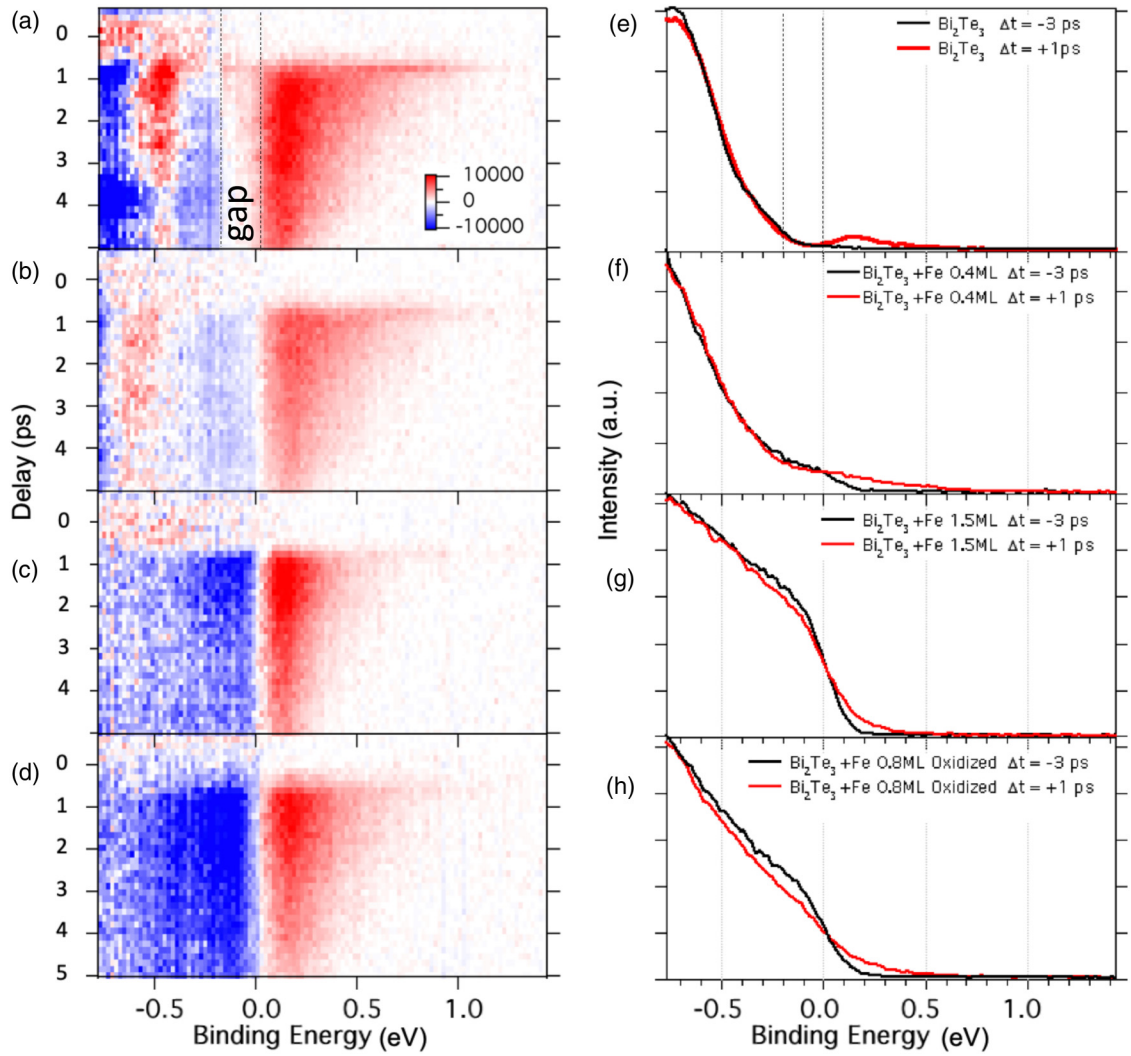

FIG. 4. Photoemission intensity map as a function of energy and delay time for Bi_2Te_3 crystal. The maps show the difference of photoelectron intensity before and after the optical excitation, for clean Bi_2Te_3 (a), capped with 0.4 ML Fe (b), capped with 1.5 ML Fe (c), and capped with 0.8 ML Fe oxidized *in situ* (d). (e)–(h) are the corresponding photoelectron energy distribution curves at 3 ps before the optical excitation (black line) and at 1 ps after the optical excitation (red line).

This small amount of iron on top of the surface does not destroy the Dirac cone, consistently with previous work [28]. The Dirac point is shifted to higher binding energy by about 200 meV and the shape of the top of the valence band (VB) is modified. We do not observe the Rashba splitting reported for Fe-capped Bi_2Te_3 [37] or Ca-capped Bi_2Se_3 compounds [38]. However, we also note that in the work of Scholz *et al.* [28] such Rashba splitting was also not observed with a similar amount of iron evaporated onto the surface of the TI. We surmise that the lack of the Rashba splitting for the exfoliated crystal could come from the cleanliness of the surface which may prevent the formation of a large enough surface built-in electric field (even if we have evidenced a band bending as discussed previously) and then limit the Rashba interaction. A low carrier concentration in the conduction band might also play a determinant role. Finally, we would like to note that the enhancement of the Rashba splitting appears to depend quite a lot on the surface dopants, their organization, and the magnetic coupling between adatoms as discussed previously in Ref. [37].

Note that we observe a drastic dependence of the photoemission cross section of Dirac states on the ARPES signal. In particular, the Dirac states which were clearly visible with a photon energy of 50 eV (UARPES) become undetectable with a photon energy of 17 eV. This has been checked both with the UARPES and HHG beamlines as shown in Supplemental Fig. 9 [29]. Consequently, the following discussion of TR-ARPES, performed with a photon energy of 17 eV, will mainly concern the bulk electronic states dynamics.

A thin BT film (15 nm) was also measured at the UARPES beamline (SOLARIS) after transfer from the MBE chamber (Chorzow) with a special cell (10^{-7} mbar) to the UARPES beamline. The band structure is shown in Fig. 2(c) and reveals the existence of Dirac states. Due to possible contamination during the transportation or due to the possible stoichiometry variation (Bi rich specimen), we observe that the thin film is naturally *n* type. Since the contrast is rather low for the static ARPES measurement obtained for the thin film (uncovered or covered), no TR-ARPES was performed for the thin film. As an alternative and complementary approach we then focused

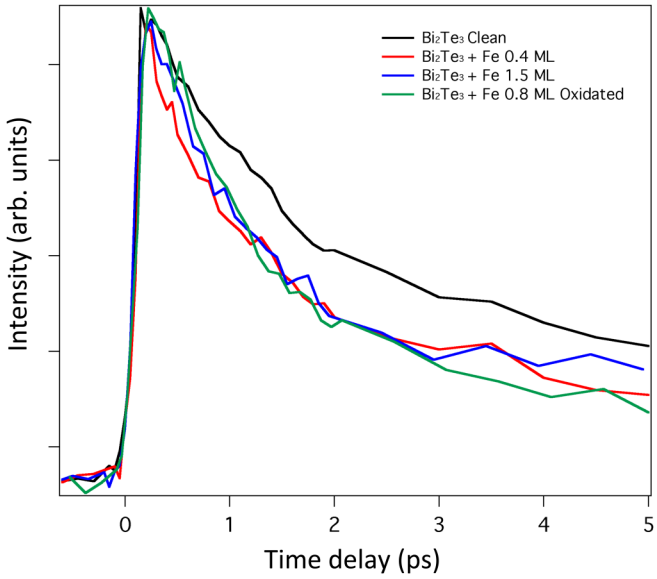

FIG. 5. Time evolution of angle and energy integrated photoemission intensity of excited states for clean Bi_2Te_3 (black line), capped with 0.4 ML Fe (red line), capped with 1.5 ML Fe (blue line), and capped with 0.8 ML Fe oxidized *in situ* (green line).

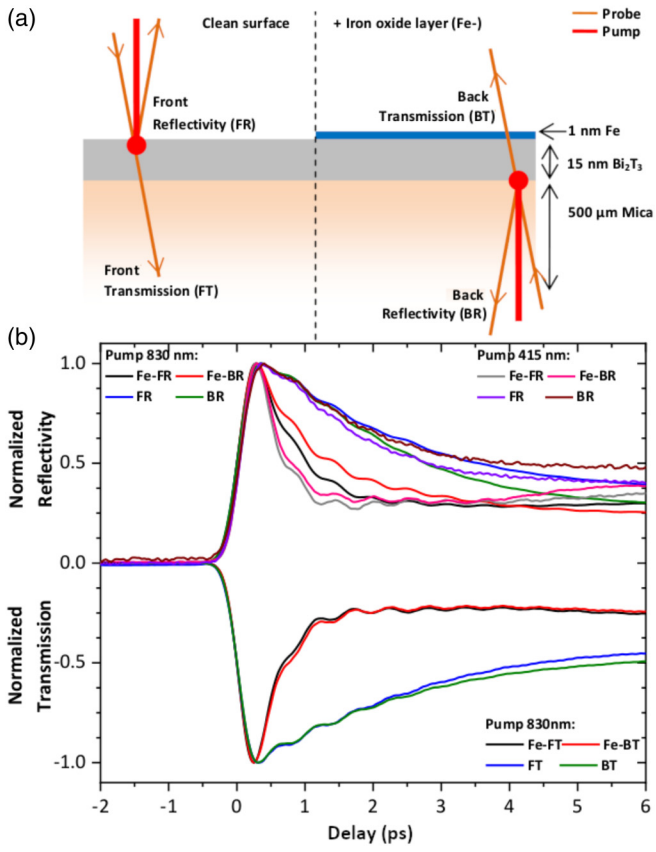

FIG. 6. (a) Configurations of the reflectivity and transmission measurements made with the sample covered partly by an iron layer. (b) Data for the two different energies of the laser beam. Time-resolved optical transmission and reflectivity obtained for the sample partly covered with Fe with a pump wavelength of 830 nm (1.49 eV) or 415 nm (2.98 eV). Signals, marked with Fe, were obtained from the part of the sample capped with iron oxide.

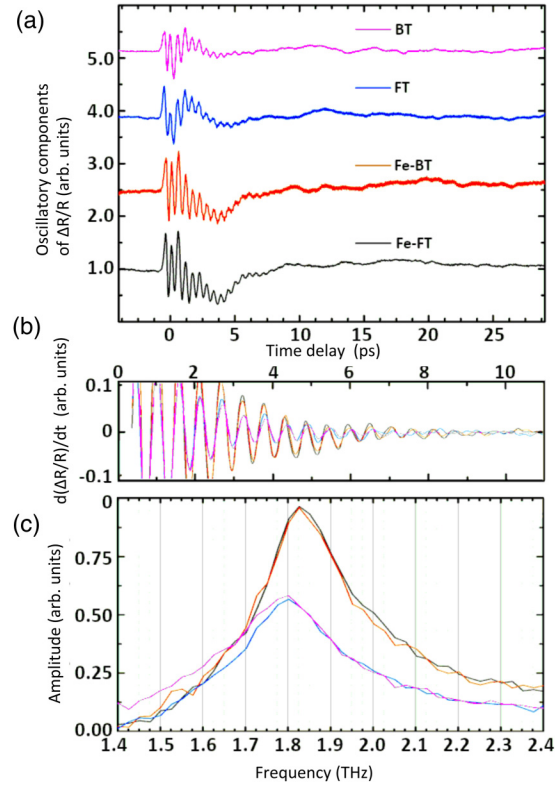

FIG. 7. (a) Phonon signal extracted from fitting of the rise and decay transient reflectivity shown in Fig. 6(b). (b) Time derivative of the transient phonon signal revealing different oscillation periods for sample with and without iron capping layer. (c) Corresponding fast Fourier transforms (FFT) of phonon signals.

our attention on the optical time-resolved ultrafast dynamics in the thin films as discussed in Sec. III D.

C. Time-resolved ARPES

The TR-ARPES measurements were performed on a single crystal at room temperature with an energy resolution of about 100 meV. The experimental conditions of our time-resolved photoemission studies do not enable us to obtain energy and angle resolution similar to the static measurement as shown in Fig. 2. As discussed previously, and whatever the sample, it appears that there is no clear Dirac cone visible both in the pre-excitation angle-resolved photoemission map (time delay −0.3 ps) and in the post-excitation Figs. 3(a)–3(c). Rather, the structure visible after excitation (time delay 2.5 ps) above the Fermi level should be mainly related to the transiently occupied conduction band. In Figs. 3(b) and 3(c), one can see a long lasting occupancy of the conduction band just above the Fermi level even for 5 ps after the pulse. This finding is in agreement with previous studies [10] where a long lifetime of excited electronic states was found.

After Fe deposition and its oxidation (see Supplemental Fig. 10 within the Supplemental Material [29]), the Dirac states were not visible. We also note that the angular distribution of the electronic states is significantly smeared out (see Supplemental Fig. 10 [29]). This is probably related to the distribution of adatoms within the spot size.

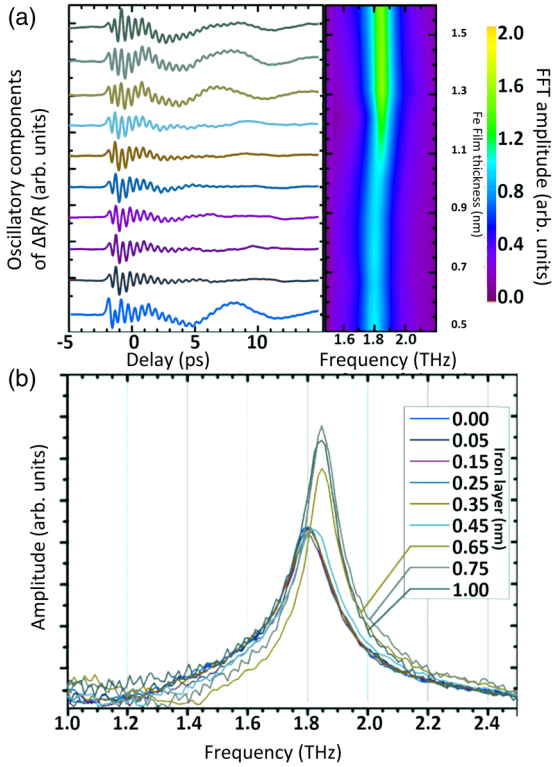

FIG. 8. (a) Phonon signal, in sample capped with a wedge of iron thin film of Bi_2Te_3, extracted after removing the electronic contribution. The corresponding FFT frequency and amplitude is given either as a map [in the right panel of (a)] or as a graphic in (b).

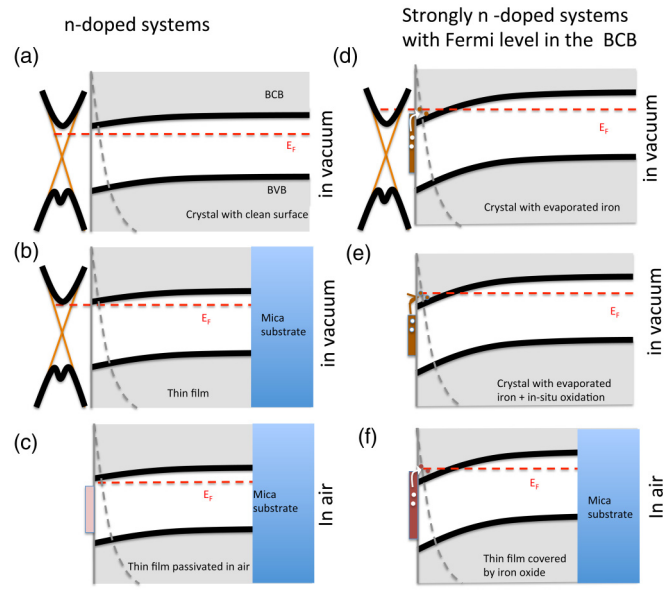

FIG. 9. Electron band structure of (a) clean Bi_2Te_3 crystal. (b) clean Bi_2Te_3 thin film. (c) 15 nm thin film of Bi_2Te_3 in air, with developed stable passivation layer of Te and Bi oxide. (d) Bi_2Te_3 crystal with a deposited capping layer of pure and (e) oxidized iron in vacuum; (f) 15 nm thin film of Bi_2Te_3 with deposited capping layer of Fe in vacuum followed by an oxidation in air. Larger band bending is observed for samples on which evaporated iron compounds was performed. The existence of Dirac states has been confirmed by ARPES only for systems shown in (a), (b), and (d) at the moment. Dashed gray curves on each figure represent the vanishing surface states with a typical extension of 2 nm as reported in the literature [48].

In order to capture the dynamics in an energy range scaling with the pump photon energy of 1.5 eV (see the definition of the region of interest (ROI), shown in Fig. 11 within the Supplemental Material [29]), angle-integrated photoemission maps were realized from Supplemental Fig. 10 given in Supplemental Material [29]. The integrated signals are shown in Figs. 4(a)–4(d). The left column, i.e., Figs. 4(a)–4(d), shows the variation of the photoemission intensity map as a function of energy and time delay for clean Bi_2Te_3, capped with 0.4 ML Fe, 1.5 ML Fe, and capped with 0.8 ML Fe and then oxidized *in situ*, respectively. The maps show the difference of photoelectron intensity before and after the excitation. Red and blue colors indicate an excess or a deficit of carriers compared to the stationary condition (thermodynamic equilibrium). The right column of Figs. 4(e)–4(h) presents the energy distribution curves (EDC) where the EDCs of the ground state and after a delay of 1 ps from the pulse are compared.

Several interesting features of the relaxation process can be found in the data collected in Fig. 4. The region of the bulk energy gap is visible only for a clean crystal for binding energies up to 200 meV [see vertical dashed blue lines in Fig. 4(a)]. The excited states are concentrated just above the Fermi level as also well illustrated by Fig. 4(e). The intensity concentrated in the region of about 100 meV above the Fermi level can be attributed to the population of the bulk conduction band. For capped specimens, we do not observe a gap but rather a clear signal revealing the existence of occupied states at the Fermi level as seen in Figs. 4(f)–4(h).

Another interesting feature which appears after excitation is the excess emission from the electronic states in the binding energy region of 400–600 meV, at the top of the valence band. That excess population of electronic states has a relatively short lifetime and it is considerably reduced after about 4 ps. Such an effect was not described earlier [9,11]. Note however that this behavior was reported for high resistance Bi_2Te_2Se (BTS) samples by Papalazarou *et al.* [14] and for Sb-doped Bi_2Te_3 (BST) samples by Sanchez-Barriga *et al.* [15] where the shift reaches typically 74 meV and 70 meV, respectively, at low temperature. This effect was attributed to a surface photovoltage (SPV). By comparing EDCs with and without pump, and within our energy resolution of 100 meV, we were not able to evidence a shift of the electronic levels as shown in Supplemental Fig. 12 [29]. This indicates a negligible SPV effect in our case. Note that the effect of excess population within the VB is still visible for a surface capped with 0.4 ML Fe and disappears for a thicker Fe layer and the oxidized surface. The last cases are consistent with the common understanding that one can expect full occupation of valence electronic states in the ground state, and an increase of the hole state population after excitation in that energy region would be expected. As the scale of the valence band energy shift remains important and larger than the SPV reported for the BST samples for instance [14], an alternative or additional possible explanation that could be taken into account is related to a transient change

TABLE I. Carrier relaxation time measured with TR-ARPES and time-resolved optical methods (reflectivity R, transmission T).

Sample/experiment	Time constant (ps)	
Bi_2Te_3 single crystal	TR-ARPES	
	τ_1	
Bi_2Te_3 clean surface	1.2 ± 0.5	
Bi_2Te_3 + Fe 0.4ML	0.49 ± 0.03	
Bi_2Te_3 + Fe 1.5 ML	1.0 ± 0.02	
Bi_2Te_3 + Fe 0.8 ML oxidated	0.90 ± 0.02	
Bi_2Te_3 thin films 15 nm	$\Delta R/R(t)$	$\Delta T/T(t)$
	τ_1	τ_1
Bi_2Te_3 Front (F)	2.09 ± 0.1	2.26 ± 0.1
Bi_2Te_3 Back (B)	1.99 ± 0.1	2.09 ± 0.1
Bi_2Te_3+Fe(1 nm) (F)	0.56 ± 0.03	0.35 ± 0.03
Bi_2Te_3+Fe(1 nm) (B)	1.05 ± 0.1	0.40 ± 0.03
Bi_2Te_3+Fe(0.8 nm) wedge (F)	0.77 ± 0.03	
Bi_2Te_3+Fe(0.5 nm) wedge (F)	1.20 ± 0.1	

of the bulk and surface electronic structure due to the excitation with the relatively high intensity 1.5 eV photon beam (1 mJ cm^{-2}). The effect of band gap modification in BT via strong photoexcitation was described by Hada *et al.* [39,40]. The transient modification of the electronic structures in TIs via photoinduced atomic motions was proposed. It is worth mentioning that the band structure of BT with antisite defects shows a strong modification of the band structure in the energy region 300–500 meV below the Fermi level [16] and there are calculations of BT electronic structure indicating the presence of the surface non-Dirac states in the binding energy range of about 400–600 meV [39,41].

Deposition of Fe (0.4 to 1.5 ML) leads to a significant increase of the density of states in the vicinity of the Fermi level [Figs. 4(f) and 4(g)]. Consistently with ARPES results shown in Fig. 2(b), we ascribe this effect to a shift of the Fermi level into the conduction band. Even if the shift of the Dirac point is toward higher binding energy, that effect is not visible in the EDCs shown in Fig. 4 as reported in previous work [28]. The reason is related to the lower energy resolution than in the spectra shown in Fig. 2(b) and to the increasing energy of the valence band offset. Oxidation of the iron layer does not change much the situation and there are still occupied levels at the Fermi level. For all hybrid nanostructures [Figs. 4(f)–4(h)], we observe a similar time evolution for holes and excited electronic states. Such so-called symmetry was shown in the paper of Sobota *et al.* [10] for *n*-type BT where the bulk electrons and holes exhibit a characteristic relaxation time of 1.67 ps and 1.85 ps, respectively. Figure 5 shows the time evolution of angle and energy integrated photoemission intensity of excited states for selected samples. The integration region is 1 eV wide, starting from the Fermi level. The curves were fitted with a multiple exponential decay function (see Supplemental Fig. 13 in the Supplemental Material [29]). The best fit was obtained for a double exponential decay model, and the results gave two time constants, indicating a faster (τ_1) and a slower process (τ_2). Values are given in Table I. While for the clean crystal the relaxation time for the faster process is about 1.2 ps, it decreases with characteristic time ranging from $\tau_1 \sim 0.4$ ps to 1 ps for the capped BT layers. This significant change of photoexcited carrier relaxation dynamics is well confirmed in capped thin film and is probed with transient optical methods described below.

D. Time-resolved optical measurements

Figure 6 shows the transient reflectivity and transmission for different configurations. The letter F (B) indicates front (back) and corresponds to an experiment where the pump beam impinges on the front of Bi_2Te_3 surface or on the back of the sample, at the interface Bi_2Te_3-mica. The probe and pump beams always impinge on the same side but the probe beam is either detected in transmission (T) or in reflection (R). Thus FT means pump excitation at the front of the sample and detection of the transient transmission and BR means pump excitation at the back of the sample and detection of the transient reflectivity [see sketch in Fig. 6(a)]. Typical signals are shown in Fig. 6(b) obtained with Fe capping (1 nm of iron oxide) (Fe-FR, Fe-BR, Fe-FT, Fe-BT) or without capping (FR, FT, BR, BT). The curves are composed of a fast decaying signal with superimposed oscillations. The oscillations (Fig. 7) are related to generated/detected Raman active optical phonons A_{1g}(I) in BT [17,19,31] that we will discuss later on. Signals in Fig. 6(b) are shown for pump photon energies of 1.49 eV and 2.98 eV. The main and clear effect is the reduction of the relaxation time for the film covered with iron oxide whatever the geometrical configuration or pump energy. As we mentioned in the Experimental Methods section, the fact that the phenomena do not depend on the pump photon energy support the view that there is a negligible effect of the contribution of optical absorption by the capping layer. For all configurations the relaxation of hot carriers, related to the electronic band structure of the films, is faster for the Fe^{3+} doped films. We have applied a fitting procedure described in Supplemental Material [29] to extract the carrier relaxation time labeled as τ_1. The results are given in Table I where we compare the values with those obtained by angle and energy integrated time-dependent photoemission signals. It is worth underlining that the relaxation time of the pure BT layer of around 2 ps measured by optical methods is in agreement with previous measurements performed with a BT crystal [39], confirming the bulklike behavior of our 15 nm thick film. In transient optical measurements, we report a larger decrease of the relaxation time by a factor of around 4 for the thicker Fe^{3+}-capping layer (1 nm). The measurements made with the wedge sample indicate that we have some intermediate values of τ_1 depending on the initial Fe capping layer thickness. For example (see Table I), we have $\tau_1 \sim 0.77$ ps and 1.2 ps for a capping layer of 0.8 nm and 0.5 nm, respectively. These results are consistent with results obtained with TR-ARPES and confirm an overall decrease of the characteristic relaxation time of photoexcited carriers when the iron "surface doping" increases, although at this stage we are not able to separate the surface and bulk carrier contributions.

It is important to discuss also the dynamics of the optically generated Raman active A_{1g}(I) mode. Once the electronic contribution is adjusted (see Supplemental Material [29]), it is possible to extract the phonon contribution superimposed on the electronic decay signal in $\Delta R/R$ [see Figs. 7(a), 7(b)

and 8(a)]. By showing that we always generate and detect this A_{1g}(I) mode, we confirm that the capping process does not modify the local symmetry of the structure (this conclusion is also supported by *in situ* and *ex situ* XPS, see Supplemental Figs. 6–9 [29]). For the sample shown in Fig. 6(a), we showed that for a 1 nm capping layer, we have a blue shift of the A_{1g}(I) phonon frequency as shown in Figs. 7(b) and 7(c). When looking at the wedge sample, we confirm that blue shift and changing the iron oxide capping layer from 0 to 1 nm leads to a nonmonotonic change of the A_{1g}(I) frequency. The frequency remains constant up to around 0.6 nm (about 3 ML) and then increases by an amount of around 5% for the thicker layer of 1 nm (5 ML) as shown in Figs. 8(a) and 8(b). Such a blue shift of a Raman active optical phonon has already been reported in the literature for rather strong photoexcitation [42–45] and was explained as a stiffening of the interatomic bonds due to a high photoexcited carrier concentration. We are not in that regime. Rather, we believe that there is such a strengthening due to a possible modification of the bond strengths by slight diffusion of some iron atoms into the film, possibly between quintuple layers. This is supported by our XPS depth profile studies shown in Supplemental Fig. 8 [29] performed with a BT film capped with the thicker 1 nm Fe layer and oxidized in air, revealing some incorporation of the iron into the film. The reason why we have a steplike function with a critical capping layer thickness of around 1 nm is not clear yet. One hypothesis, yet to be confirmed, relies on the formation of FeTe alloy in the first layers, and once such an alloy is formed, the additional iron atoms preferentially migrate in the film along the columnar grains revealed in Ref. [26] to be finally incorporated in the van der Waals planes between quintuple layers of BT.

E. Discussion

The ARPES and TR-ARPES measurements (EDCs) performed on a single BT crystal show that when covered by a couple of iron MLs, the Fermi level is shifted within the conduction band, and that effect can be modulated by the amount of deposited iron. Our *in situ* XPS analysis (Fig. 1(a) and Supplemental Figs. 2 and 5 [29]) also indicate a shift towards higher binding energy for the Te $3d$ and Bi $4f$ core levels by about 0.2 eV which is close to the energy shift seen in Fig. 2(b). These observations favor a downward band bending effect. Without extrapolating straightforwardly the physics of junctions to our hybrid nanostructures, we note that considering the work function of 4.6–5.1 eV [46] for Bi_2Te_3 [47] and of 4.3 eV for iron, we can expect a band bending towards higher binding energy and a shift of the Fermi level in the conduction which is in agreement with our observation in Fig. 2(b). A sketch of the proposed band bending is shown in Fig. 9 for the different systems we have investigated. Of course the chemical interaction of some elements at the interface has also to be taken into account and the junction might not be ideal. In our case, chemical reaction was found in the XPS spectra indicating some possible formation of FeTe at the interface and the appearance of metallic Bi for the covered BT crystal (see the XPS spectra shown in Supplemental Figs. 2–5 [29]). The same tendency is observed for the *in situ* oxidized iron capped BT crystal with a clear relation between the Fermi level shift in the conduction band (EDCs in Fig. 4) and the observation of a signature of a band bending with XPS measurements (Fig. 1(a) and Supplemental Figs. 2 and 3 [29])

Such band bending and the associated shift of the Fermi level in the conduction band observed in the BT crystal covered by iron or iron oxide appears to be quite robust since we did not detect any SPV within the range of pump fluence investigated and within our energy resolution. The presence of the Fermi level in the CB is a favorable situation for bulk photoexcited carriers to thermalize through new energy and momentum relaxation channels accessible for both the surface and bulk out-of-equilibrium electrons. For a Fermi level shifted into the CB, the hot carrier dynamics indeed approaches the metallic situation where fast intraband processes take place.

Such behavior is also expected to be at play in thin BT films capped with iron oxide. Although no ARPES and TR-ARPES were performed for thin films capped with iron oxide, the XPS measurements show a similar signature of a band bending (see Fig. 1(b) and Supplemental Fig. 5 [29]). It is worth mentioning that the film of Bi_2Te_3, without evaporation of iron, but passivated in air does not exhibit a detectable core level shift in the XPS signals, as already discussed in a previous paper [19]. This indicates that similarly to the clean BT crystal, no drastic band bending effect is expected as sketched in Fig. 9(c). The capping layer of thin films is more complex, with various oxides (see Supplemental Figs. 6 and 7 [29]), but still also exhibits an energy shift towards higher binding energy of the Te $3d$ and Bi $4f$ levels. Finally, with transient optical measurements, we clearly evidence the decrease of the relaxation time, consistently with the results observed for the BT crystal capped with iron oxide. There is, however, an important difference between bulk and thin films. For the latter, the carrier relaxation time is much more reduced (see Table I) since we have a reduction by a factor ranging from 4 to 7 depending on the capping layer thickness and the characteristic relaxation time approaches that of large electron-phonon coupling metals [49]. It is worth noting that, contrary to ARPES measurements which are sensitive to the first layers (1–2 nm), the transient optical dynamics of hot carriers probed either in reflection or in transmission is a response of the material measured over the optical skin depths of pump and probe, i.e., over a typical depth of 6–10 nm [50] which scales with the film thickness. Consequently, we have to consider that such a drastic decrease of the relaxation time might exist in the entire film and is not limited to scattering processes at an interface. Such an optical signal integrates both the surface and the bulk states' responses without allowing separation of the contributions. The significant decrease of the relaxation time might have two origins. First of all, it is likely that the band bending and the Fermi shift concern nearly the entire film and is not limited to the first layers at the interface. This is consistent with estimates obtained in the related compound Bi_2Se_3 where, with a band bending energy shift of 0.2–0.26 eV [27], i.e., similar to the one we observe in Bi_2Te_3 (see Fig. 1(b) and Supplemental Fig. 5 [29]), the extension of the depletion layer is around 20 nm [27], so of the same order as the film thickness. As mentioned before for the case of the crystal, having a Fermi level in the CB favors fast intraband relaxation processes. (Remark: we note that

the band at the interface BT/mica can be expected to remain flat due to the limited interaction with the van der Waals surface of mica). The second possible reason to explain the drastic decrease of the relaxation time is based on the role of defects. For a thick capping iron oxide layer, we also show the presence of diffusion of iron into the film for a capping layer as thick as 1 nm. Besides the modification of the interatomic bond strength revealed by the blue shift of the Raman active mode A_{1g}(I) (Figs. 7 and 8), such diffusion of iron atoms can create some new levels in the electronic structure, that can contribute to the increase of scattering of hot carriers, even if at the moment we cannot quantify the effect.

IV. SUMMARY AND CONCLUSIONS

Deposition of Fe on the surface of a crystal of the model 3D topological insulator leads to several interesting phenomena. For very low coverage, up to about 1 ML, the electronic structure is modified and the conduction band is partially filled but the Dirac surface states are still present. Even such a low coverage has a clear impact on the electronic structure by shifting the Fermi level into the conduction band (donor effect). We observe then a significant decrease in the lifetime of photoexcited carriers (at least, bulk carriers) by TR-ARPES. With an iron oxide capping layer we observe the same tendency of an electron donor effect and the subsequent reduction of the hot carrier relaxation time. The transient optical measurements performed with thin film of Bi_2Te_3 covered by iron oxide, also show this behavior with a reduction of the hot carrier relaxation time by a factor ranging from 2 to 7 depending on the amount of iron oxide on the surface.

The general behavior, and the basis of the ARPES and XPS analysis of the electronic structure of our systems, suggests the deposition of iron or iron oxide might lead to the creation of a junction with an associated band bending and a significant shift of the Fermi level into the conduction band. In some cases, a reaction of Fe with BT was observed leading to formation of metallic Bi and probably FeTe but it is limited to the interface. The drastic bulk hot carrier dynamics change is observed in nearly the entire thin film which has a thickness of 15 nm, so suggesting indeed that the effect of the capping layer on the electronic band structure extends over several nanometers. We can qualitatively explain the evolution of the carrier dynamics as a consequence of an increase of the intraband scattering process efficiency due to the increase of the metallicity of the system illustrated by the significant shift of the Fermi level in the conduction band. We note that such drastic evolution of the carrier dynamics is at least partly attributed to the bulk electronic states, although we do not claim at this stage that Dirac states exhibit the same behavior.

Our results also show that by detecting the Raman active coherent phonon A_{1g}(I) dynamics, we demonstrate that the local symmetry is not broken. Furthermore, a careful analysis of this optical phonon mode frequency shows it evolves with the capping layer thickness, and we suggest that there exists a limit of around 1 nm (5 ML) for the capping layer over which some diffusion of iron atoms takes place within the BT layer. In that situation the interface and the junction effect can become more complicated even if the overall effect on the photoexcited carriers is to drastically reduce their lifetime.

These results demonstrate that both chemical and physical aspects of such a junction have to be understood to control in the future the injection of spin current. Even if we probe at the moment mainly the photoexcited bulk carrier dynamics, we can anticipate that such efficient channels of relaxation for hot carriers might also have some importance in the spin-to-charge conversion process involving the Dirac surface states that will be interesting to check experimentally in the future.

ACKNOWLEDGMENTS

Partial financial support from the Polish National Science Center under Project No. 2016/21/B/ST5/02531 is acknowledged. This work was supported by the Central European Research Infrastructure Consortium, CERIC-ERIC, under the internal research project Dyna Chiro. This work has received funding from the European Union's Horizon 2020 research and innovation programme under Grant Agreement No. 654360 NFFA-Europe. We also acknowledge the support of the ARRS Project No. ARRS-RPROJ-VP-2021/74. M.W. thanks the French Embassy in Poland for the PhD grant and Polish National Science Center for the research Grant No. 2017/25/N/ST3/01806. This work was supported by the French Ministry of Education and Research, the CNRS, and Region Pays de la Loire (CPER Femtosecond Spectroscopy equipment program).

[1] J. E. Moore and L. Balents, Topological invariants of time-reversal-invariant band structures, Phys. Rev. B **75**, 121306(R) (2007).

[2] J. E. Moore, The birth of topological insulators, Nature (London) **464**, 194 (2010).

[3] M. Z. Hasan and C. L. Kane, Colloquium: Topological insulators, Rev. Mod. Phys. **82**, 3045 (2010).

[4] W. Han, Y. C. Otani, and S. Maekawa, Quantum materials for spin and charge conversion, npj Quantum Mater. **3**, 27 (2018).

[5] S. Zhang and A. Fert, Conversion between spin and charge currents with topological insulators, Phys. Rev. B **94**, 184423 (2016).

[6] J.-C. Rojas-Sánchez, S. Oyarzún, Y. Fu, A. Marty, C. Vergnaud, S. Gambarelli, L. Vila, M. Jamet, Y. Ohtsubo, A. Taleb-Ibrahimi, P. Le Fèvre, F. Bertran, N. Reyren, J.-M. George, and A. Fert, Spin to Charge Conversion at Room Temperature by Spin Pumping into a New Type of Topological Insulator: α-Sn Films, Phys. Rev. Lett. **116**, 096602 (2016).

[7] X. Wang, L. Cheng, D. Zhu, Y. Wu, M. Chen, Y. Wang, D. Zhao, C. B. Boothroyd, Y. M. Lam, J.-X. Zhu, M. Battiato, J. C. W. Song, H. Yang, and E. E. M. Chia, Ultrafast spin-to-charge conversion at the surface of topological insulator thin films, Adv. Mater. **30**, e1802356 (2018).

[8] D. Hsieh, F. Mahmood, J. W. McIver, D. R. Gardner, Y. S. Lee, and N. Gedik, Selective Probing of Photoinduced Charge and Spin Dynamics in the Bulk and Surface of a Topological Insulator, Phys. Rev. Lett. **107**, 077401 (2011).

[9] J. A. Sobota, S.-L. Yang, D. Leuenberger, A. F. Kemper, J. G. Analytis, I. R. Fisher, P. S. Kirchmann, T. P. Devereaux, and Z.-X. Shen, Distinguishing Bulk and Surface Electron-Phonon Coupling in the Topological Insulator Bi_2Se_3 Using Time-Resolved Photoemission Spectroscopy, Phys. Rev. Lett. **113**, 157401 (2014).

[10] J. A. Sobota, S. Yang, J. G. Analytis, Y. L. Chen, I. R. Fisher, P. S. Kirchmann, and Z.-X. Shen, Ultrafast Optical Excitation of a Persistent Surface-State Population in the Topological Insulator Bi_2Se_3, Phys. Rev. Lett. **108**, 117403 (2012).

[11] M. Hajlaoui, E. Papalazarou, J. Mauchain, G. Lantz, N. Moisan, D. Boschetto, Z. Jiang, I. Miotkowski, Y. P. Chen, A. Taleb-Ibrahimi, L. Perfetti, and M. Marsi, Ultrafast surface carrier dynamics in the topological insulator Bi_2Te_3, Nano Lett. **12**, 3532 (2012).

[12] S. Ciocys, T. Morimoto, R. Mori, K. Gotlieb, Z. Hussain, J. G. Analytis, J. E. Moore, and A. Lanzara, Manipulating long-lived topological surface photovoltage in bulk-insulating topological insulators Bi_2Se_3 and Bi_2Te_3, npj Quantum Mater. **5**, 16 (2020).

[13] M. Neupane, S.-Y. Xu, Y. Ishida, S. Jia, B. M. Fregoso, C. Liu, I. Belopolski, G. Bian, N. Alidoust, T. Durakiewicz, V. Galitski, S. Shin, R. J. Cava, and M. Z. Hasan, Gigantic Surface Lifetime of an Intrinsic Topological Insulator, Phys. Rev. Lett. **115**, 116801 (2015).

[14] E. Papalazarou, L. Khalil, M. Caputo, L. Perfetti, N. Nilforoushan, H. Deng, Z. Chen, S. Zhao, A. Taleb-Ibrahimi, M. Konczykowski, A. Hruban, A. Wolos, A. Materna, L. Krusin-Elbaum, and M. Marsi, Unraveling the Dirac fermion dynamics of the bulk-insulating topological system Bi_2Te_2Se, Phys. Rev. Mater. **2**, 104202 (2018).

[15] J. Sánchez-Barriga, M. Battiato, E. Golias, A. Varykhalov, L. V. Yashina, O. Kornilov, and O. Rader, Laser-induced persistent photovoltage on the surface of a ternary topological insulator at room temperature, Appl. Phys. Lett. **110**, 141605 (2017).

[16] J. A. Sobota, S.-L. Yang, D. Leuenberger, A. F. Kemper, J. G. Analytis, I. R. Fisher, P. S. Kirchmann, T. P. Devereaux, and Z.-X. Shen, Ultrafast electron dynamics in the topological insulator Bi_2Se_3 studied by time-resolved photoemission spectroscopy, J. Elec. Spec. Relat. Phenom. **195**, 249 (2014).

[17] M. Weis, K. Balin, R. Rapacz, A. Nowak, M. Lejman, J. Szade, and P. Ruello, Ultrafast light-induced coherent optical and acoustic phonons in few quintuple layers of the topological insulator Bi_2Te_3, Phys. Rev. B **92**, 014301 (2015).

[18] Y. D. Glinka, S. Babakiray, T. A. Johnson, A. D. Bristow, M. B. Holcomb, and D. Lederman, Ultrafast carrier dynamics in thin-films of the topological insulator Bi_2Se_3, Appl. Phys. Lett. **103**, 151903 (2013).

[19] M. Weis, B. Wilk, G. Vaudel, K. Balin, R. Rapacz, A. Bulou, B. Arnaud, J. Szade, and P. Ruello, Quantum size effect on charges and phonons ultrafast dynamics in atomically controlled nanolayers of topological insulators Bi_2Te_3, Sci. Rep. **7**, 13782 (2017).

[20] S. Kim, D. H. Shin, J. H. Kim, C. W. Jang, J. W. Park, H. Lee, S.-H. Choi, S. H. Kim, K.-J. Yee, N. Bansal, and S. Oh, Resonance effects in thickness-dependent ultrafast carrier and phonon dynamics of topological insulator Bi_2Se_3, Nanotechnology **27**, 045705 (2016).

[21] L. Braun, G. Mussler, A. Hruban, M. Konczykowski, T. Schumann, M. Wolf, M. Munzenberg, L. Perfetti, and T. Kampfrath, Ultrafast photocurrents at the surface of the three-dimensional topological insulator Bi_2Se_3, Nat. Commun. **7**, 13259 (2016).

[22] F. Vidal, M. Eddrief, B. R. Salles, I. Vobornik, E. Velez-Fort, G. Panaccione, and M. Marangolo, Photon energy dependence of circular dichroism in angle-resolved photoemission spectroscopy of Bi_2Se_3 Dirac states, Phys. Rev. B **88**, 241410(R) (2013).

[23] Y. Zhang, K. He, C.-Z. Chang, C. L. Song, L.-L. Wang, X. Chen, J.-F. Jia, Z. Fang, X. Dai, W.-Y. Shan, S.-Q. Shen, Q. Niu, X.-L. Qi, S.-C. Zhang, X.-C. Ma, and Q.-K. Xue, Crossover of the three-dimensional topological insulator Bi_2Se_3 to the two-dimensional limit, Nat. Phys. **6**, 584 (2010).

[24] Y. Y. Li, G. Wang, X. G. Zhu, M. H. Liu, C. Ye, X. Chen, Y. Y. Wang, K. He, L. L. Wang, X. C. Ma, H. J. Zhang, X. Dai, Z. Fang, X. C. Xie, Y. Liu, X. L. Qi, J. F. Jia, S. C. Zhang, and Q. K. Xue, Intrinsic topological insulator Bi_2Te_3 thin films on Si and their thickness limit, Adv. Mater. **22**, 4002 (2010).

[25] J. Zhang, J. P. Velex, X. Dang, and E. Y. Tsymbal, Band structure and spin texture of Bi_2Se_3 3d ferromagnetic metal interface, Phys. Rev. B **94**, 014435 (2016).

[26] K. Balin, R. Rapacz, M. Weis, and J. Szade, Physicochemical analysis of (Fe, Eu)Bi_2Te_3 junctions grown by molecular beam epitaxy method, AIP Adv. **7**, 056323 (2017).

[27] C. E. ViolBarbosa, C. Shekhar, B. Yan, S. Ouardi, E. Ikenaga, G. H. Fecher, and C. Felser, Direct observation of band bending in the topological insulator Bi_2Se_3, Phys. Rev. B **88**, 195128 (2013).

[28] M. R. Scholz, J. Sanchez-Barriga, D. Marchenko, A. Varykhalov, A. Volykhov, L. V. Yashina, and O. Rader, Tolerance of Topological Surface States towards Magnetic Moments: Fe on Bi_2Se_3, Phys. Rev. Lett. **108**, 256810 (2012).

[29] See Supplemental Material at http://link.aps.org/supplemental/10.1103/PhysRevB.104.245110 for (a) description of samples under investigation (Supplemental Fig. 1), (b) XPS data (Supplemental Figs. 2–8), (c) time resolved ARPES data (Supplemental Figs. 9–12), (d) extraction of the relaxation time in time-resolved ARPES (Supplemental Fig. 13) and time-resolved optical measurements [51].

[30] QUASES-IMFP-TPP2M program by S. Tougaard, http://www.quases.com/home/.

[31] K. Balin, M. Wojtyniak, M. Weis, M. Zubko, B. Wilk, R. Gu, P. Ruello, and J. Szade, Europium doping impact on the properties of MBE Grown Bi_2Te_3 thin film, Materials **13**, 3111 (2020).

[32] C. Grazioli, C. Callegari, A. Ciavardini, M. Coreno, F. Frassetto, D. Gauthier, D. Golob, R. Ivanov, A. Kivimaki, B. Mahieu, B. Bucar, M. Merhar, P. Miotti, L. Poletto, E. Polo, B. Ressel, C. Spezzani, and G. De Ninno, CITIUS: An infrared-extreme ultraviolet light source for fundamental and applied ultrafast science, Rev. Sci. Instrum. **85**, 023104 (2014).

[33] F. Frassetto and L. Poletto, Grating configurations to compress extreme-ultraviolet ultrashort pulses, App. Optics **54**, 7985 (2015).

[34] A. G. Joly, J. R. Williams, S. A. Chambers, G. Xiong, and W. P. Hess, Carrier dynamics in α-Fe2O3 (0001) thin films and

single crystals probed by femtosecond transient absorption and reflectivity, J. Appl. Phys. **99**, 053521 (2006).

[35] R. Grau-Crespo, A. Y. Al-Baitai, I. Saadoune, and N. H. De Leeuw, Vacancy ordering and electronic structure of γ-Fe_2O_3 (maghemite): a theoretical investigation, J. Phys.: Condens. Matter **22**, 255401 (2010).

[36] G. V. Hansson and R. I. G. Uhrberg, Photoelectron spectroscopy of surface states on semiconductor surfaces, Surf. Sci. Rep. **9**, 197 (1988).

[37] L. A. Wray, S.-Y. Xu, Y. Xia, D. Hsieh, A. V. Fedorov, Y. S. Hor, R. J. Cava, A. Bansil, H. Lin, and M. Z. Hasan, A topological insulator surface under strong Coulomb, magnetic and disorder perturbations, Nat. Phys. **7**, 32 (2011).

[38] P. D. C. King, R. C. Hatch, M. Bianchi, R. Ovsyannikov, C. Lupulescu, G. Landolt, B. Slomski, J. H. Dil, D. Guan, J. L. Mi, E. D. L. Rienks, J. Fink, A. Lindblad, S. Svensson, S. Bao, G. Balakrishnan, B. B. Iversen, J. Osterwalder, W. Eberhardt, F. Baumberger, and Ph. Hofmann, Large Tunable Rashba Spin Splitting of a Two-Dimensional Electron Gas in Bi_2Se_3, Phys. Rev. Lett. **107**, 096802 (2011).

[39] D. Hsieh, Y. Xia, D. Qian, L. Wray, F. Meier, J. H. Dil, J. Osterwalder, L. Patthey, A. V. Fedorov, H. Lin, A. Bansil, D. Grauer, Y. S. Hor, R. J. Cava, and M. Z. Hasan, Observation of Time-Reversal-Protected Single-Dirac-Cone Topological-Insulator States in Bi_2Te_3 and Sb_2Te_3, Phys. Rev. Lett. **103**, 146401 (2009).

[40] M. Hada, K. Norimatsu, S. Tanaka, S. Keskin, T. Tsuruta, K. Igarashi, T. Ishikawa, Y. Kayanuma, R. J. D. Miller, K. Onda, T. Sasagawa, S.-Y. Koshihara, and K. G. Nakamura, Bandgap modulation in photoexcited topological insulator Bi_2Te_3 via atomic displacements, J. Chem. Phys. **145**, 024504 (2016).

[41] P.-Y. Chuang, S.-H. Su, C.-W. Chong, Y.-F. Chen, Y.-H. Chou, J.-C.-A. Huang, W.-C. Chen, C.-M. Cheng, K.-D. Tsuei, C.-H. Wang, Y.-W. Yang, Y.-F. Liao, S.-C. Weng, J.-F. Lee, Y.-K. Lan, S.-L. Chang, C.-H. Lee, C.-K. Yang, H.-L. Suh, and Y.-C. Wu, Anti-site defect effect on the electronic structure of a Bi_2Te_3 topological insulator, RSC Adv. **8**, 423 (2018).

[42] R. Ernstorfer, M. Harb, C. T. Hebeisen, G. Sciaini, T. Dartigalongue, and R. J. D. Miller, The formation of warm dense matter: experimental evidence for electronic bond hardening in gold, Science **323**, 1033 (2009).

[43] H. Yan, D. Song, K. F. Mak, I. Chatzakis, J. Maultzsch, and T. F. Heinz, Time-resolved Raman spectroscopy of optical phonons in graphite: Phonon anharmonic coupling and anomalous stiffening, Phys. Rev. B **80**, 121403(R) (2009).

[44] G. Lantz, B. Mansart, D. Grieger, D. Boschetto, N. Nilforoushan, E. Papalazarou, N. Moisan, L. Perfetti, V. L. R. Jacques, D. Le Bolloc'h, C. Laulhe, S. Ravy, J.-P. Rueff, T. E. Glover, M. P. Hertlein, Z. Hussain, S. Song, M. Chollet, M. Fabrizio, and M. Marsi, Ultrafast evolution and transient phases of a prototype out-of-equilibrium Mott-Hubbard material, Nat. Commun. **8**, 13917 (2017).

[45] D. Boschetto, L. Malard, C. H. Lui, K. F. Mak, Z. Li, H. Yan, and T. F. Heinz, Real-time observation of interlayer vibrations in bilayer and few-layer graphene, Nano Lett. **13**, 46204623 (2013).

[46] G. N. Derry, M. E. Kern, and E. H. Worth, Recommended values of clean metal surface work functions, J. Vac. Sci. Technol. A **33**, 060801 (2015).

[47] D. Haneman, Photoelectric emission and work functions of InSb, GaAs, Bi, Te and Germanium, J. Phys. Chem. Solids **11**, 205 (1959).

[48] S. Giraud, A. Kundu, and R. Egger, Electron-phonon scattering in topological insulator thin films, Phys. Rev. B **85**, 035441 (2012).

[49] S. D. Brorson, A. Kazeroonian, J. S. Moodera, D. W. Face, T. K. Cheng, E. P. Ippen, M. S. Dresselhaus, and G. Dresselhaus, Femtosecond Room-Temperature Measurement of the Electron-Phonon Coupling Constant λ in Metallic Superconductors, Phys. Rev. Lett. **64**, 2172 (1990).

[50] D. M. Greenaway and G. Harbere, Band structure of bismuth telluride and their alloys, J. Phys. Chem. Solids **26**, 1585 (1965).

[51] N. Mouton, M. Sliwa, G. Buntinx, and C. Ruckebusch, Deconvolution of femtosecond time-resolved spectroscopy data in multivariate curve resolution. Application to the characterization of ultrafast photo-induced intramolecular proton transfer, Chemometrics **24**, 424 (2010).